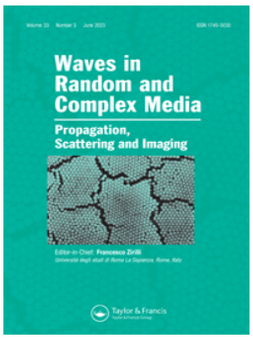

Taylor & Francis
Taylor & Francis Group

Waves in Random and Complex Media

ISSN: (Print) (Online) Journal homepage: https://www.tandfonline.com/loi/twrm20

The broadband absorber based on plasma metastructure with spiral resonators

Haining Ye, Li Zeng, Baofei Wan & Haifeng Zhang

To cite this article: Haining Ye, Li Zeng, Baofei Wan & Haifeng Zhang (2023): The broadband absorber based on plasma metastructure with spiral resonators, Waves in Random and Complex Media, DOI: 10.1080/17455030.2023.2222848

To link to this article: https://doi.org/10.1080/17455030.2023.2222848

Published online: 09 Jun 2023.

WAVES IN RANDOM AND COMPLEX MEDIA
https://doi.org/10.1080/17455030.2023.2222848

The broadband absorber based on plasma metastructure with spiral resonators

Haining Ye, Li Zeng, Baofei Wan and Haifeng Zhang

College of Electronic and Optical Engineering & College of Flexible Electronics (Future Technology), Nanjing University of Posts and Telecommunications, Nanjing, People's Republic of China

ABSTRACT

In this paper, firstly, a dual narrowband absorber based on plasma metastructure with a single spiral resonator is proposed, whose absorption rate in the frequency bands of 19.60 ~ 20.21 GHz and 23.08 ~ 25.55 GHz is higher than 90%. Through continuous optimization, a broadband absorber composed of four spiral structures with different sizes is finally obtained. When the absorption is larger than 90%, the absorption frequency domain of this absorber can cover from 21.11 to 28.08 GHz, with a relative bandwidth of 28.3%. What's more, the absorption principle of spiral absorber has also been studied in the process of parameter discussion in depth. The design process of this absorber also contributes to a new approach for expanding the operation bandwidths of other similar ones. Compared with the conventional absorbers, the proposed device is more compact, and superior in absorption, with the designable electromagnetic parameters of the material. In addition, the given absorber has exceedingly extensive application prospects in the fields of detection, imaging, and electromagnetic stealth.

ARTICLE HISTORY
Received 5 October 2022
Accepted 2 May 2023

KEYWORDS
Metastructure; absorber; solid plasma; spiral resonators; broadband absorption

1. Introduction

Metamaterial (MM), an artificial periodic structure whose unit size is remarkably smaller than its operating wavelength, is usually composed of basic resonant units [1]. Through the precise micro-geometry design of its resonant unit, the MM can present a string of peculiar electromagnetic properties, including negative refractive index [2], reverse Doppler effect [3], and so on, which are not possessed by natural materials. Simultaneously, metastructures (MSs) with essentially similar principles to MM, are three-dimensional (3D) topologies, and easier to integrate in contrast with traditional natural materials, making them better adapt to the development of contemporary technology. In fact, MS is a concept derived from MMs [4]. To be specific, MS represents the evolution of multi-layer structures, two-dimensional metasurfaces or 3D topology, and other variable structures, which generally has superior performance to simple MM units. Hitherto, the increasing complexity of application scenarios and the pursuit of devices with superior performance have brought the implementation of MSs to the forefront. In particular, the metastructure absorber (MSA)

CONTACT Haifeng Zhang hanlor@163.com

is a significant branch with rapid growth in the field of MS. It is the bright prospects of MSAs in electromagnetic compatibility [5], stealth technology [6], and other aspects that urge them to arouse widespread attention.

At present, there are considerable research results in the exploration of MSAs, including perfect absorbers [7], multi-frequency absorbers [8], broadband absorbers [9], tunable absorbers [10], etc. In 2008, a nearly perfect absorber was put forward by Landy et al., whose absorption rate is as high as 96% at the operating frequency of 11.6 GHz [7]. Subsequently, inspired by the design concept of Landy, a variety of MSAs with broad band have been designed, simulated, and implemented, with the frequency bands studied extended to terahertz (THz), near-infrared, and visible light. At the same time, multi-frequency absorbers originated single-frequency absorbers have been gradually realized. Tianhua et al. came up with and theoretically studied a simple five-band perfect MSA in THz region, performing absorption peaks at five resonant frequencies whose peaks average 98.85% [11]. Moreover, the broadband MSA is one of the research hotspots for the reason that the realization of broadband absorption is propitious to practical application. Using multilayer structure [12], loading lumped elements [13], designing planar multi-size resonant units [14] and other methods can effectively expand the absorption frequency band. By making full use of the square-ring dielectric multi-layer absorption structure, a broadband absorber was implemented by Xiong et al., presenting strong absorption characteristics in the frequency range of 8.37 $\sim$ 21.90 GHz [15]. With lumping elements loaded, a new type of broadband MSA including four-wheel resonators of different sizes was confirmed by Karaaslan et al. [16]. A six-band MSA composed of four multi-mode Ω-shaped resonators was proposed by Xu et al., provided with six distinct near-perfect absorption peaks from 2 to 17 GHz [17]. Utilizing indium-tin-oxide films, Deng et al. have proposed the ultrawide and polarization-insensitive MSA, working from 10 $\sim$ 75.5 GHz [18]. A year later, they put forward a new ultra-broadband MSA by making advantage of water substrate and dielectric-resonator [19].

Apart from adopting complex structural design methods, all kinds of materials emerging in an endless stream, are also tried to be applied to superior MSAs. Among these various materials, solid plasma is a type of significant material with outstanding advantages, such as tunable electromagnetic properties, high working frequency, and ease of integration [20]. Since the formation of solid plasma can be dominated by external voltages, Kong et al. ingeniously exploited this property to investigate a tunable polarization-independent MSA based on solid plasma, operating in the THz band [21]. A broadband absorber integrating solid plasma with a frequency-selective surface and covering the X – and Ku-bands was reported by Joozdani et al. [22]. Besides the change of material, the shape of the resonance unit of the MSA is also constantly innovating. And it is worth pointing out that spiral structures endowed with plenty of merits, such as angular stability and polarization insensitivity, are extensively used in the construction of absorbers. Hua et al. proposed a multi-frequency MSA with the top layer consisting of four identical spiral metal wires. Due to the quadruple rotational symmetry of the spiral resonator, the electromagnetic response is insensitive to the polarization of the incident wave [23]. Simultaneously, the performance of the spiral MSA in terms of angular stability of the angle of incidence cannot be underestimated after elaborate engineering. For instance, an optically transparent microwave MSA was demonstrated by Shi et al. [24]. An impedance layer composed of a square spiral unit cell is utilized to enhance microwave absorption for the sake of angular stability of eminence. The novel

Table 1. Summary of specific structural parameters involved in the MSA 1.

Parameter	P	R	r	d	H	h_1	h_2
Value (mm)	18	5.7	0.85	0.42	1.5	0.1	0.1

spiral structure evolved, transformed, and processed from the basic spiral structure has also injected new vitality into the progress and improvement of the MSAs.

K-band refers to the frequency band of electromagnetic wave (EMW) 18 ~ 27 GHz, which is a military band mainly used in radar communication and mobile satellite communication [25]. Currently, a growing body of countries focuses on the development and application of K-band broadband satellite communications, which is the grounds that the MSAs in this paper are designed in this frequency band.

Based on the above content, a spiral broadband MSA is formulated in this paper. This work realizes dual-band absorption by a single spiral structure at the beginning. By arranging four spiral structures that evolved from single spiral structure with different geometric dimensions in an array and making certain changes, the bandwidth (BW) of the original single spiral absorber has been significantly expanded. This method of increasing BW is universal and reproducible, which offers references and means for similar structures to optimize BW. Additionally, the absorption mechanism and performance of the optimized MSA are also discussed and analyzed in detail.

2. Structure design

The structure diagram of the single spiral narrowband MSA consisting of a three-layer structure is drawn in Figure 1. Aimed to ensure that EMW rarely reflects, the bottom layer is a metal plate made of copper with a conductivity σ of 5.8×10^7 S/m [26]. And the top layer is a solid plasma Archimedes spiral. Describing with the Drude model, the dielectric constant of the solid plasma is expressed as $\varepsilon_p(\omega) = \varepsilon_{\infty} - \omega_p^2 / (\omega^2 + j\omega\omega_c)$, where the ε_{∞} is 12.4, the solid plasma frequency $\omega_p$is 2.9×10^{14} rad/s, and the solid plasma collision frequency is 1.65×10^{13} rad/s [27].

For the Archimedes spiral, α denotes the radius ratio (the ratio of the longest radius R of the spiral to the shortest radius r, expressed by the calculation formula as $\alpha = R/r$). In this single spiral absorber with the definition of MSA 1, α and the width of spiral d are 6.7 and 0.85, respectively. Besides, another representative parameter of the spiral is the number of revolutions N, which is taken as 5 in this resonator. The metal plate and the spiral are separated by a layer of FR-4 (the relative permittivity $\varepsilon = 4.3$, and the dielectric loss tangent is 0.025) [28]. To be more intuitive, the structural parameters of MSA 1 are summarized in Table 1.

Figure 1(a2) – (e2) show a schematic diagram of the structure of the MSA with four spirals as resonant units, which is defined as MSA 2. The four spiral structures are numbered accordingly in the order shown in Figure 1(a1). The spirals ①, ②, ③, and ④ are all obtained from the single spiral in Figure 1 through scaling, translation, and rotation. The spirals ④, ③, ②, and ① are rotated counterclockwise around the center by a certain angle relative to the original spiral, which is 0°, 90°, 180°, and 270°, respectively, which can avoid the sensitivity to the polarization of EMW to a certain extent. Among them, k_1, k_2, k_3, and k_4 represent

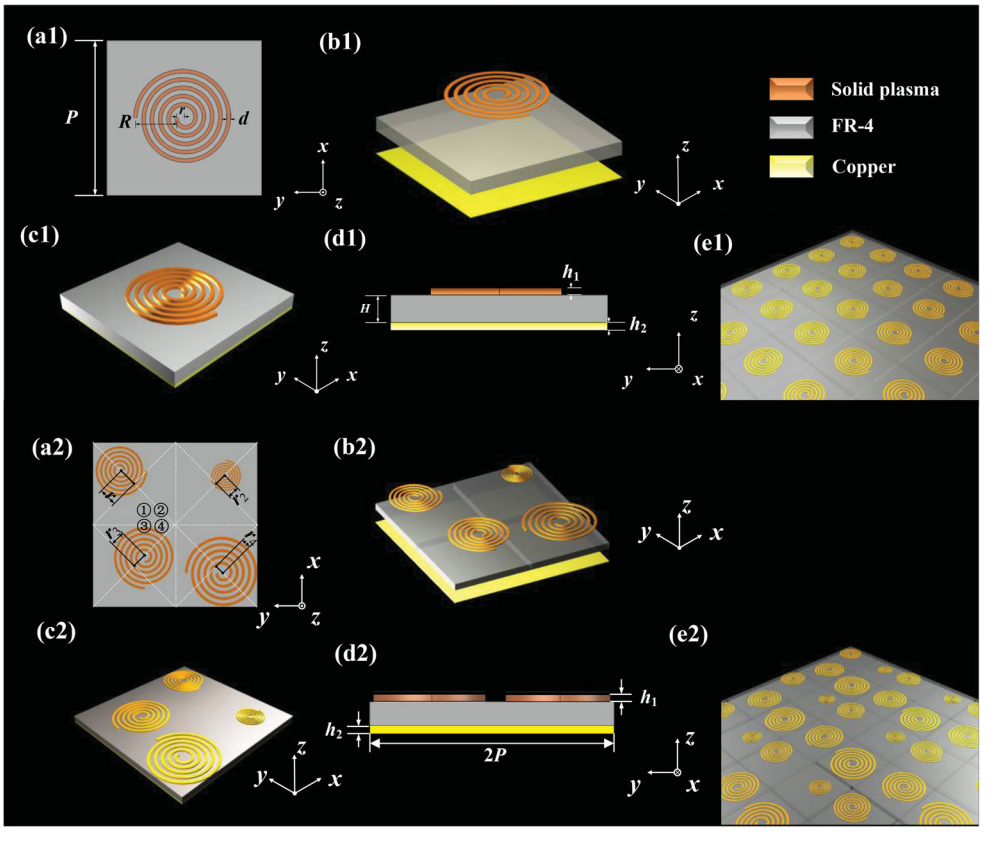

Figure 1. The structure diagrams of MSA 1 and MSA 2: (a1) the planform of the MSA 1, (b1) the structural separation diagram of the MSA 1, (c1) the graphic model of the MSA 1, (d1) the side elevation of the MSA 1, (e1) schematic diagram of periodic surface composed of MSA 1, (a2) the planform of the MSA 2, (b2) the structural separation diagram of the MSA 2, (c2) the graphic model of the MSA 2, (d2) the side elevation of the MSA 2, and (e2) schematic diagram of periodic surface composed of MSA 2.

Table 2. Summary of the specific structural parameters involved in MSA 2.

Parameter	r_1	r_2	r_3	r_4	k_1	k_2	k_3	k_4
Valu e (mm)	$3\sqrt{2}$	$2\sqrt{2}$	$2\sqrt{2}$	$\sqrt{2}$	1	0.6	1.2	1.4

the proportional scaling ratios of the spirals ①, ②, ③, and ④ relative to the original spiral structure, respectively. Moreover, $\boldsymbol{r_1}$, $\boldsymbol{r_2}$, $\boldsymbol{r_3}$, and $\boldsymbol{r_4}$ delegate the translation distances of the spirals ①, ②, ③, and ④ along the diagonal 45° from the center of the unit. The corresponding parameters during the change are summarized in Table 2 to describe MSA 2 more clearly.

3. Simulation results and analyze

Numerical simulation is carried out in the commercial software High Frequency Structure Simulator (HFSS), the polarized EMW is vertically incident on the MS surface along the –

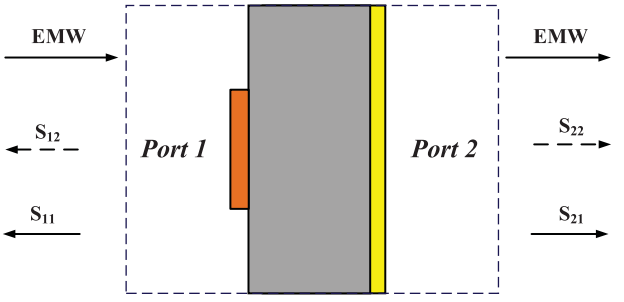

Figure 2. Schematic representation of the S-parameters.

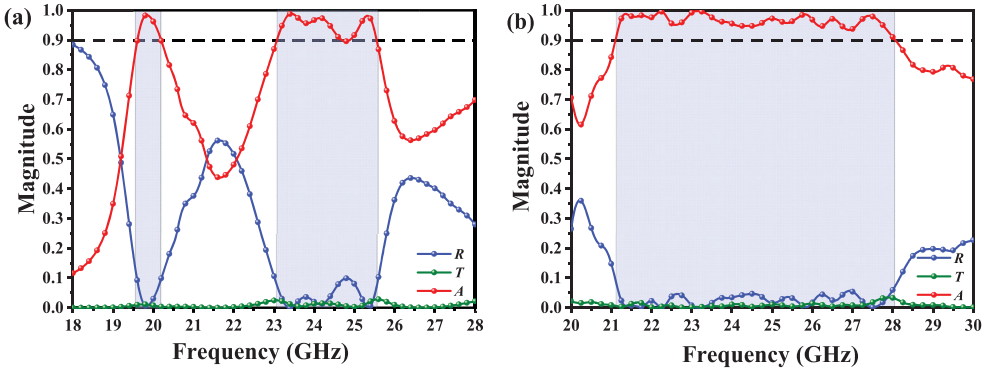

Figure 3. Reflection, transmission and absorption spectra: (a) the MSA 1, and (b) the MSA 2.

z-direction, and the master-slave boundary and the Floquet port are set to simulate the periodic boundary and EMW incidence, respectively.

Considering that the bottom plate of the MSA is made of pure copper, it can be approximated that EMW cannot be transmitted through, which leads to the result that the transmittance $\boldsymbol{T}$ is 0. Therefore, in Figure 2, $A(\omega)$ can be expressed in terms of S-parameters but also in terms of reflectivity $\boldsymbol{R}$, that is [29–35]:

$$A = 1 - |S_{11}|^2 - |S_{21}|^2 = 1 - R \tag{1}$$

The absorption, reflection, and transmission spectra of MSA 1 for the transverse-electric (TE) polarization (the electric field is parallel to the *x*-axis) under the normal incidence are respectively displayed in Figure 3(a) [36]. In Figure 4, the MSA 1 is a dual-narrowband absorber, whose absorption rate in the two frequency bands of 19.58 ~ 20.17 GHz and 23.08 ~ 25.54 GHz is higher than 90%, with 1.6% and 10.1% relative bandwidths (RBs), respectively. There is high-efficiency absorption within a certain range. However, the fly in the ointment is that the BW is narrow. Due to the continuous metal backplane for the MSA, the transmission is almost 0, which again proves the correctness of Eq. (1).

Aimed at broadband absorption, MSA 2 is finally obtained by synthesizing the analysis of several crucial factors such as the revolutions $\boldsymbol{N}$ of the spiral resonator, the thickness $\boldsymbol{H}$ of the dielectric layer, and the thickness $\boldsymbol{h}_1$ of the solid plasma, and optimizing the arrangement. The specific MS of the optimized absorber is displayed in Figure 1. The absorption rate is

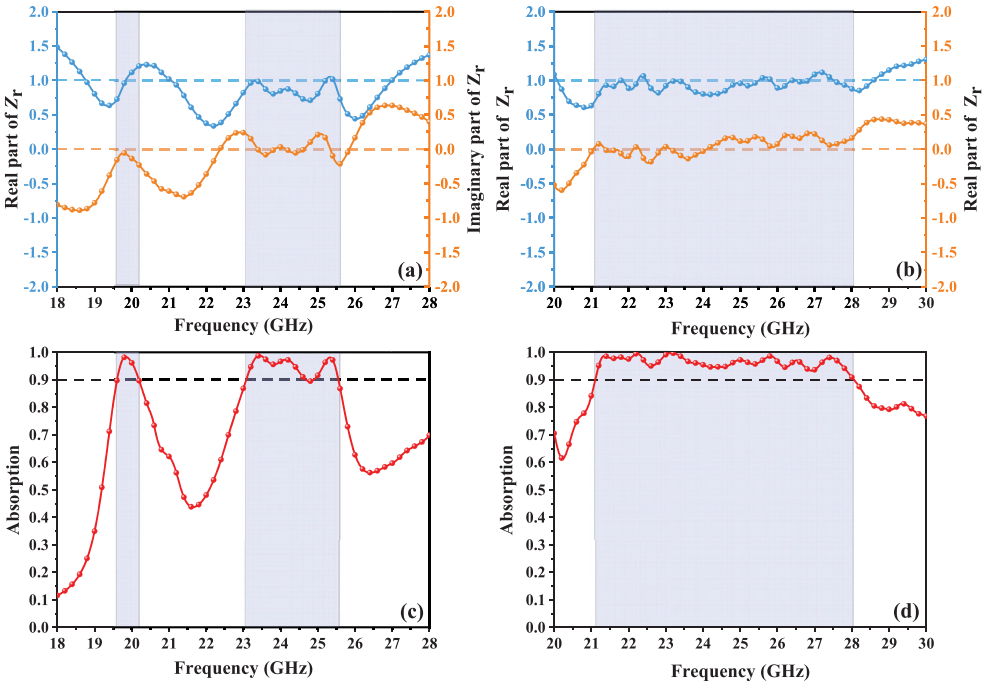

Figure 4. Absorption, real parts and imaginary parts of the relative impedance Z_r of spectra: (a) real parts and imaginary parts of the relative impedance Z_r of MSA 1, (b) real parts and imaginary parts of the relative impedance Z_r of MSA 2, (c) absorption of MSA 1, and (d) absorption of MSA 1.

carried out and shown in Figure 3(b). It can be concluded that the MSA 2 has accomplished an absorption rate larger than 90% in the range of 21.11 ~ 28.08 GHz, with 28.3% RB. Especially at 22.24 and 23.13 GHz, the absorption is almost 1, which can be considered perfect absorption and there is almost no EMW reflection or transmission. Compared with MSA 1, the absorption BW has significantly broadened. In practical application, it is accepted that the RB is higher than 20%, that is, the broadband, so it is rational to draw the conclusion that the MSA 2 has achieved broadband absorption [37].

The principles of impedance matching demand to be introduced in order to elucidate the physical mechanism of the remarkable optimization of absorption performance from MSA 1 to MSA 2. When the EMW is under normal incidence, the relationship between ***A*** and the relative impedance Z_r can be described as [38–42]:

$$A = 1 - R = 1 - \left|\frac{Z - Z_0}{Z + Z_0}\right|^2 = 1 - \left|\frac{Z_r - 1}{Z_r + 1}\right|^2 \tag{2}$$

$$Z_r = \pm\sqrt{\frac{(1 + S_{11})^2 - S_{21}{}^2}{(1 - S_{11})^2 - S_{21}{}^2}} \tag{3}$$

Where $Z_r = Z/Z_0$ means the relative impedance between the MSA and the free space and $Z_0 = 377\ \Omega$ stands for the wave impedance in vacuum. It is deduced that when Z matches Z_0, $Z_r = Z/Z_0 = 1$, leading the consequence that the absorption reaches the maximum. Specifically, the real part of Z_r is close to 1 at this time, while the imaginary part

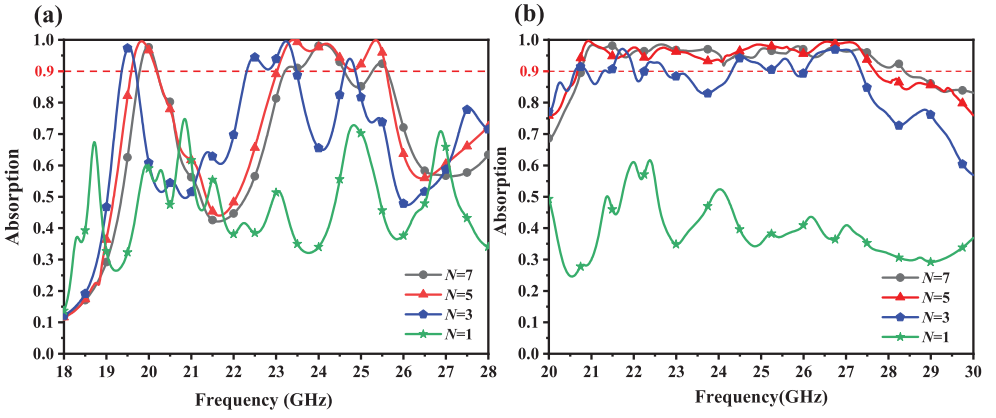

Figure 5. The absorption spectra when the revolutions **N** changes:(a) MSA 1, and (b) MSA 2.

approaches 0. There are the real and imaginary parts of Z_r and the absorption of MSA 1 and MSA 2 curves in Figure 4. It is apparent to speculate from Figure 5 that the absorption performance of MSA 2 is significantly superior to that of MSA 1 with respect to ***A*** and absorption BW, mainly since the impedance in MSA 2 is matched better with the impedance of free space.

For the spiral resonator, the number of revolutions ***N*** of the spiral is a vital parameter. Therefore, in the parameter discussion, the absorption rates under different ***N*** values in MSA 1 and MSA 2 are firstly computed in Figure 5(a) and (b). Comprehensively viewing the analysis of these two figures, it is logical to conclude that ***N*** imposes the similar effect on the two kinds of the absorber. In general, the absorption also enhanced distinctively as ***N*** is increasing. When $\boldsymbol{N} = 5$, the absorption performance of MSA 1 is significantly better than the other circumstances, occupied with the wider BW and three perfect absorption peaks at the same time. As for MSA 2, the absorbers with $\boldsymbol{N} = 7$ and $\boldsymbol{N} = 5$ have their own merits. The absorber with $\boldsymbol{N} = 7$ encompasses a wider working frequency band, specifically 20.75 ∼ 28.37 GHz. And while $\boldsymbol{N} = 5$, the average absorption rate is higher.

In the case of the same number of revolutions, the different radius ratio $\boldsymbol{\alpha}$ also plays a crucial role in the size of the spiral, thus it has an obvious effect on the absorption performance of the MSA. In Figure 6, the curves of absorption varying with $\boldsymbol{\alpha}$ show that the larger the radius ratio, that is, the larger the spiral, the better the absorption performance will be. Considering the absorption performance of MSA 1 and MSA 2 comprehensively, the final radius ratio of 6.7 is selected in this design, so that both MSAs have the wider BW.

In addition to the revolutions ***N*** and radius ratio $\boldsymbol{\alpha}$, the solid plasma thickness $\boldsymbol{h_1}$ of the spiral structure is also one of the staple parameters that may affect absorption performance. Therefore, the corresponding circumstances of the parameters in MSA 1 and MSA 2 are also simulated and can be seen in Figure 7. It can be inferred that $\boldsymbol{h_1}$ varying between 0.05 ∼ 0.2 mm exerts a slight impact on the absorption performance of the two MSAs. For MSA 1, obviously, the absorption rate with thicker solid plasma is also larger where the absorption rate is higher than 90%. Hence, a solid plasma thickness of 0.1 mm is adopted in this article, which is a reasonable choice with taking the absorption performance and the thickness of the structure into account simultaneously. Of course, on some specific occasions, it is also rational to choose a thicker solid plasma appropriately to pursue the ultimate

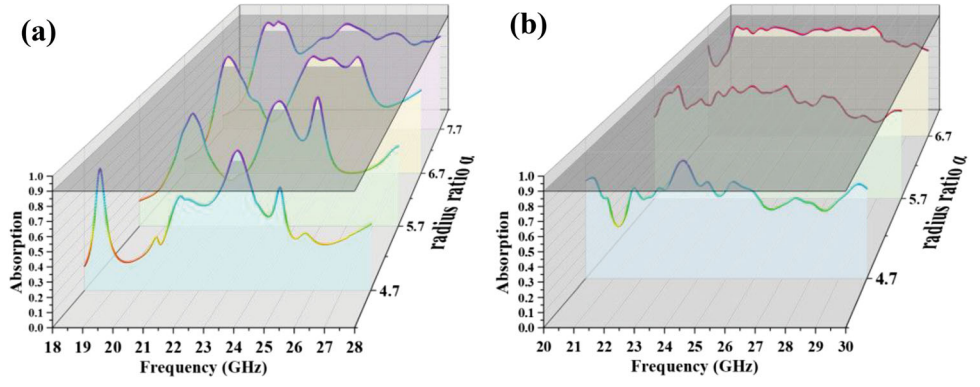

Figure 6. The absorption spectra when the radius ratio α changes:(a) MSA 1, and (b) MSA 2.

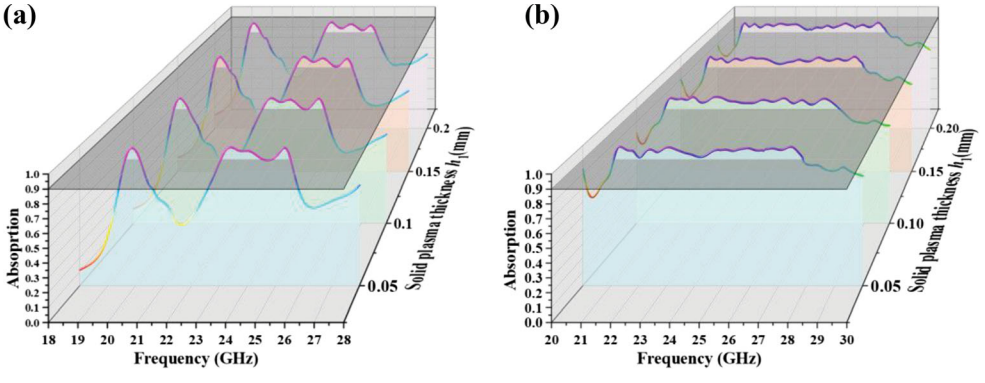

Figure 7. The absorption spectra when the solid plasma thickness h_1 changes:(a) MSA 1, and (b) MSA 2.

absorption properties. For MSA 2, when h_1 is 0.1 mm, two perfect absorption peaks perform better, which is unique and not found in other thicknesses of the MSAs.

The relationship between the structural parameter H (the thickness of dielectric layer) and the absorption spectra of MSA 1 and MSA 2 are given in Figure 8(a) and (b), respectively. As can be seen from Figure 8, H is a momentous parameter affecting the performance of MSA 1, which is manifested in that not only does it have a non-trivial effect on the position of two absorption frequency bands, but the BWs are also affected by H. With the increasing of H, the working band will move in the low-frequency direction. For instance, the working frequency band at $H = 1$ mm is significantly higher than the operating band at $H = 1.75$ mm, shifting to high frequency by about 3 GHz. For the sake of the widest possible RB of MSA 1, the setting of $H = 1.5$ mm is adopted in the conclusion. Meanwhile, the structural parameter H of MSA 2 and its relationship with the absorption spectra are plotted in Figure 8(b). Similar to the case of MSA 1, the thickness of the dielectric layer is also an extremely significant parameter able to affect the performance of MSA 2. The operating band will move to the low-frequency direction as H increases. Besides, it is worth noting that H exerts a spanking conspicuous effect on the absorption rate at the same time. When $H = 1$ mm, there is only one absorption peak of MSA 2 whose absorption is higher than 0.9. In sharp contrast, the absorption range of MSA 2 with $H = 1.5$ mm covers from 21.11 GHz to 28.08 GHz,

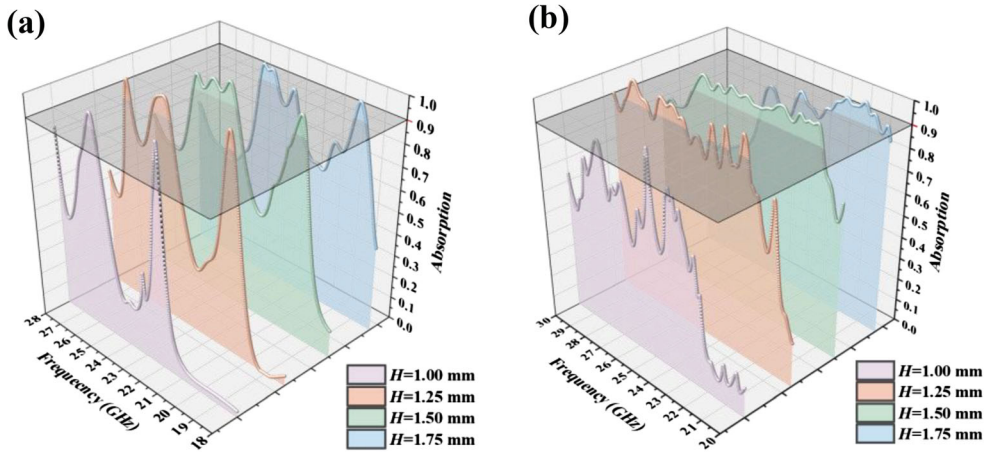

Figure 8. Absorption spectra when dielectric layer thickness ***H*** changes:(a) MSA 1, (b) MSA 2.

which happens to belong to the ***K***-band. This phenomenon reveals that the loss of EMW in the dielectric layer is likely to be one of the vital factors for the broadband absorption of MSA 2. This is why a precise comparison of MSA 2 using lossy dielectric and lossless dielectric respectively is made in the following text.

In practice, EMW is usually an oblique incident into the MSA so the incidence angle θ of EMW is a concerning factor. And the absorption versus incident angle θ is shown in Figure 9. When the EMW is incident vertically, that is, when θ is 0°, the MSA 2 has the best absorption properties. The absorptive character of MSA 2 is sensitive to the change in the incident angle. θ becoming larger, the absorption BW is obviously reduced, with the absorption rate getting smaller. The effect of polarization angle φ on the MSA is also not negligible apart from θ, which is used in discussion about the polarization sensitivity (Figure 10). Therefore, Figure 11 displays the simulation results under different polarization of incident EMW. In comparison with the incident angle θ, the MSA 2 is slightly insensitive to the change of polarization angle φ, which can be mainly attributed to the certain rotational symmetry of spirals. When φ increases, the absorption performance of the MSA 2 will deteriorate, but the reduction can be tolerated. When φ is 40°, the absorption rate is less than 0.9 in only a minor part of the frequency band.

To analyze the physical mechanism of the MSA 2, Figure 11 displays the distribution map of electric field of the dielectric substrate with a thickness of 1.5 mm and the surface current map of the metal reflector plate (at the frequency points 22.24 and 23.13 GHz, where the absorber has realized perfect absorption). Figure 11(a) and (c) are the electric field distribution figures of the upper surface of the MSA 2 at 22.24 and 23.13 GHz, respectively when θ of EMW is 0°. At this time, the electric field of MSA 2 is mainly distributed in the dielectric substrate and the edge of the spiral structure (as shown by '○' in the figure). It can be concluded that the broadband absorption of MSA 2 is mainly due to the effect of dielectric resonance. The incident EMW propagates through the solid plasma resonance unit on the surface of the dielectric substrate, and the energy of the EMW is lost in the dielectric substrate (lossy FR-4), thus obtaining the effect of absorbing the EMW. The electric field is mainly distributed on the edge and outside of the spiral, as can be seen in Figure 11(a). It is reasonable to equate

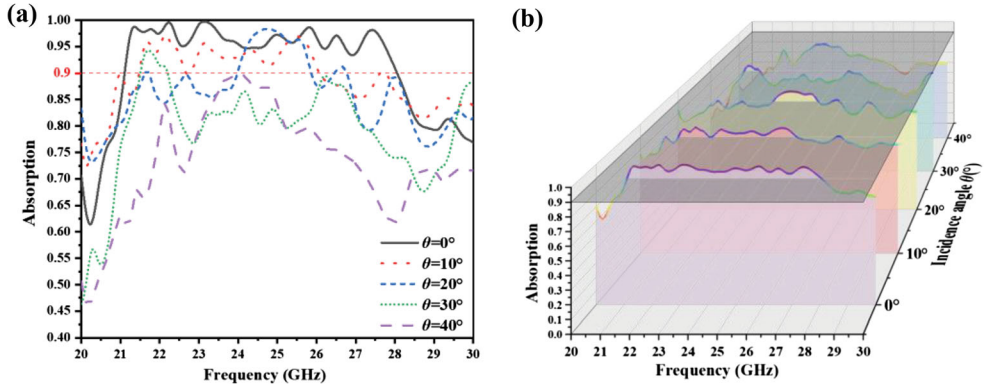

Figure 9. Absorption spectra with different incidence angles θ:(a) waterfall plot, (b) curve plot.

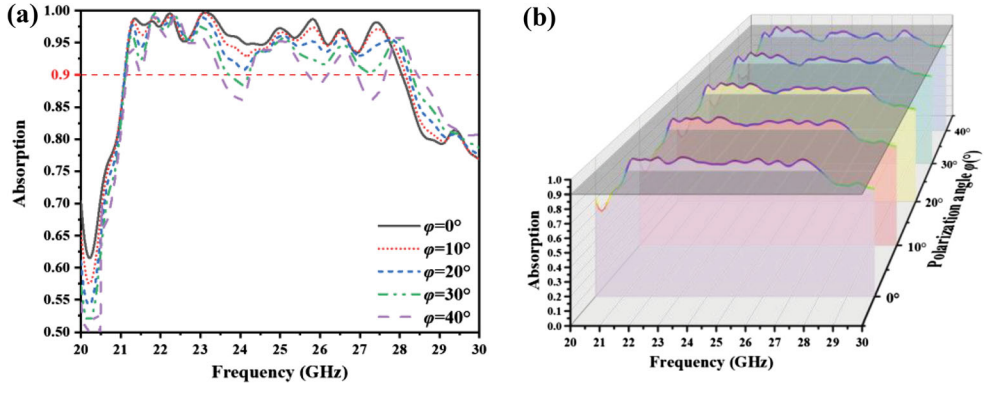

Figure 10. Absorption spectra with different polarization angles φ:(a) waterfall plot, (b) curve plot.

the upper surface of the absorber to a positive charge. As shown in Figure 11(b), the surface current on the bottom metal plate flows in the direction indicated by the arrow, which can be equivalent to the existence of a negative charge on the metal bottom plate of MSA 2. Therefore, the upper and lower surfaces can be regarded as electric dipoles, forming a magnetic resonance between them. This magnetic resonance will be coupled with the external incident EMW so that the energy of the incident EMW will be wasted in the dielectric substrate. A similar phenomenon can be seen in Figure 11(c) and (d). Obviously, it is shown that the top and bottom layers can be regarded as electric dipoles capable of generating magnetic resonances, thereby dissipating the energy of incident EMW.

On this basis, the EMW loss mechanism of the MSA 2 is further studied. Figure 12 shows the lossy and lossless time-consuming absorption spectra of the dielectric substrate. In addition, the energy loss density maps of the upper surface at the frequency points 22.24 and 23.13 GHz are also given in Figure 13(a) and (b), respectively. When the dielectric substrate (FR-4) is lossless, there is only one absorption peak whose absorption is close to 1, followed by a significant decrease in the absorption performance of MSA 2 without broadband absorption. Therefore, there is no doubt that dielectric substrate loss is one of the capital sources of absorption.

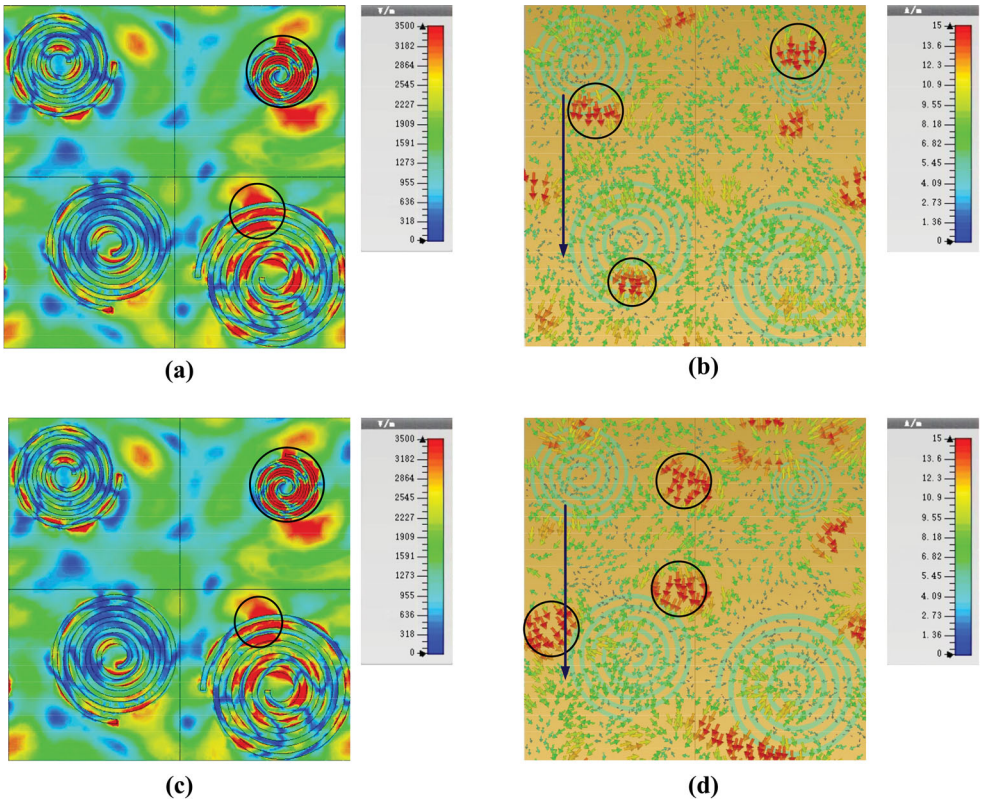

Figure 11. The electric field and surface current diagrams of the upper surface of the MSA 2 at different frequency points: (a) electric field diagram at frequency point 22.24 GHz, (b) surface current diagram at frequency point 22.24 GHz, (c) electric field diagram at frequency point 23.12 GHz, (d) electric field diagram at frequency point 23.12 GHz, (d) surface current diagram at 13.73 GHz.

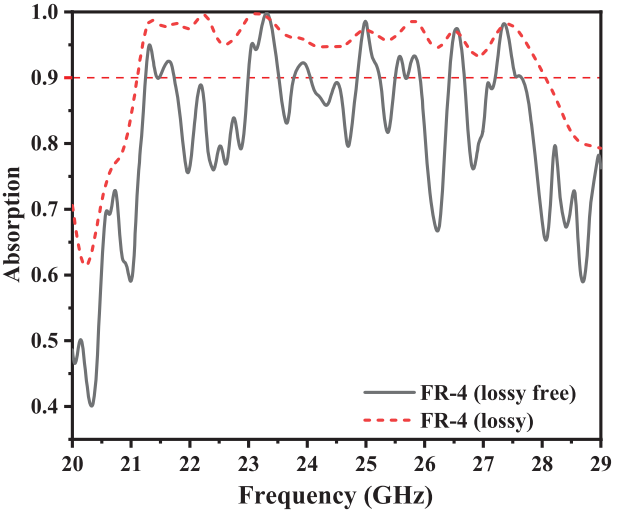

Figure 12. Absorption spectra of MSA 2 with different dielectric loss.

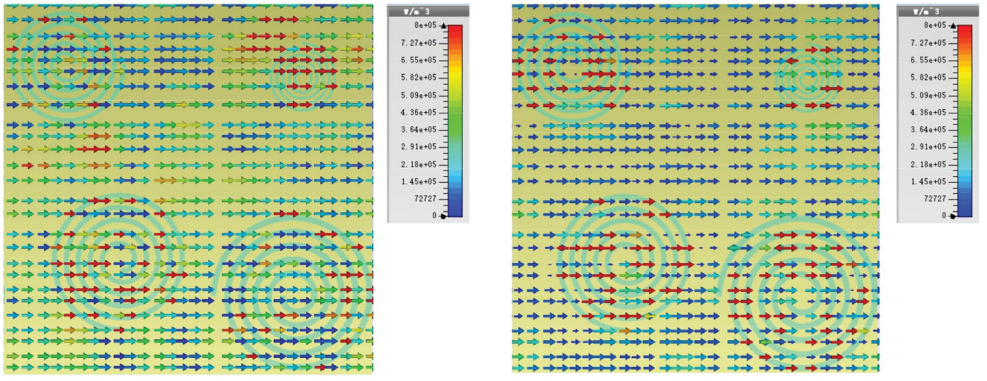

Figure 13. The energy loss density diagrams of the upper surface of MSA 2 at different frequencies: (a) energy loss density diagram at 22.24 GHz, and (b) energy loss density diagram at 23.12 GHz.

Table 3. Comparisons between this work and reported broadband MSAs.

Reference	Size	Thickness	Operating regime and performance	Relative bandwidth
[43]	2.4 μm × 2.4 μm	40 nm	105–114 THz, $A_c > 90\%$	About 8.2%
[44]	40 mm × 40 mm	6 mm	7.3–8 GHz, $A_c > 90\%$	About 9.2%
[45]	6 mm × 6 mm	2.2 mm	Around 6.2–8 GHz, $A_c > 90\%$	About 25.3%
[46]	332 μm × 332 μm	114 μm	0.565–0.578 THz, $A_c > 90\%$	About 22.7%
[47]	28 μm × 28 μm	5.3 μm	3.5–4 THz, $A_c > 90\%$	About 13.3%
This work	36 mm × 36 mm	1.5 mm	21.11–28.08 GHz, $A_c > 90\%$	About 28.3%

As can be seen from Figure 13(a) and (b), the energy loss of incident EMW is mainly distributed on the inner side of the spiral structure. In contrast with the energy loss density at the frequency point 22.24 GHz, the energy loss at the frequency point 23.12 GHz is lower, indicating that the MSA consumes more electromagnetic energy at low frequencies. Based on the above analysis and consideration, the energy of the incident EMW is mainly lost by the solid plasma resonance unit on the surface of the dielectric substrate and the dielectric substrate.

Finally, in order to highlight the novelty of this work more clearly, the previously reported absorbent devices are summarized and listed in Table 3 for comparison. In this paper, a diverse approach that the realization of broadband MSA is via the combination of four distinct cell structures is taken.

4. Conclusion

In this work, a double narrowband MSA with solid plasma based on a single spiral structure is firstly proposed, and its absorption rate is higher than 90% in both the 19.60 ~ 20.21 GHz and 23.08 ~ 25.55 GHz frequency bands. Through the continuous optimization of the design scheme, a broadband absorber composed of four spiral structures of different sizes is finally designed. When the absorption rate is higher than 90%, the absorption frequency domain of the MSA can cover from 21.11 to 28.08 GHz, and the RB is 28.3%. In addition, in the process of in-depth discussion of parameters, several key parameters such as the ratio

of the single-spiral MSA, the thicknesses of the dielectric layer, and solid plasma are also discussed. By analyzing the electric field distribution, surface current, and energy loss diagrams of the MSA, the results show that the energy loss of the MSA for EMW is mainly caused by the dielectric and magnetic resonances. The process of optimization also provides a new way to extend the BW of other MSAs of similar structures. Compared with traditional devices, the proposed MSA is simple in structure, superior in absorption performance, and the electromagnetic parameters of the material can be designed. In addition, the broadband MSA has extremely broad application prospects in the fields of detection, imaging, and electromagnetic stealth.

Disclosure statement

No potential conflict of interest was reported by the author(s).

References

[1] Kalraiya S, Chaudhary R K, Abdalla M A. Resistor loaded wideband conformal metamaterial absorber for curved surfaces application. AEU: Arch fur Elektron Ubertrag: Electron Commun. 2022;143:154033.
[2] Borazjani O, Naser-Moghadasi M, Rashed-Mohassel J, et al. Design and fabrication of a new high gain multilayer negative refractive index metamaterial antenna for X-band applications. Int J RF Microw Comput-Aided Eng. 2020;30(9): doi:10.1002/mmce.22284
[3] Liu C, Long H, Zhou C, et al. Reversed Doppler effect based on hybridized acoustic Mie resonances. Sci Rep. 2020;10(1):1519–1525. doi:10.1038/s41598-020-58370-3
[4] Qiao P, Yang W, Chang-Hasnain CJ. Recent advances in high-contrast metastructures, metasurfaces, and photonic crystals. Adv Opt Photonics. 2018;10(1):180–245. doi:10.1364/AOP.10.000180
[5] Chaurasiya D, Ghosh S, Bhattacharyya S, et al. Compact multi-band polarisation-insensitive metamaterial absorber. Iet Microw Antennas Propag. 2016;10(1):94–101. doi:10.1049/iet-map.2015.0220
[6] Mengyu S, Chen X, Zhihong Y, et al. Achieving good infrared-radar compatible stealth property on metamaterial-based absorber by controlling the floating rate of Al type infrared coating. J Alloys Compd. 2018;764:314–322. doi:10.1016/j.jallcom.2018.06.093
[7] Landy N I, Sajuyigbe S, Mock JJ, et al. A perfect metamaterial absorber. Phys Rev Lett. 2008;100(20):207402.
[8] Kalraiya S, Chaudhary RK. Polarization independent triple band ultrathin conformal metamaterial absorber for C- and X-frequency bands. AEU: Arch fur Elektron Ubertrag: Electron Commun. 2021;135(1):153752.
[9] Romero-García V, Theocharis G, Richoux O, et al. Use of complex frequency plane to design broadband and sub-wavelength absorbers. J Acoust Soc Am. 2016;139(6):3395. doi:10.1121/1.4950708
[10] Yao G, Ling F, Yue J, et al. Dual-band tunable perfect metamaterial absorber in the THz range. Opt Express. 2016;24(2):1518–1527. doi:10.1364/OE.24.001518
[11] Tianhua M, Dan H, Hongyan W, et al. Theoretical investigation of a five-band terahertz absorber based on an asymmetric split-ring resonator. Appl Opt. 2017;56(34):9601. doi:10.1364/AO.56.009601
[12] Liu S, Chen H, Cui T J. A broadband terahertz absorber using multi-layer stacked bars. Appl Phys Lett. 2015;106(15):163702–163478.
[13] Karaaslan M, Bamanc M, ünal E, et al. Broad band metamaterial absorber based on wheel resonators with lumped elements for microwave energy harvesting. Opt Quantum Electron. 2018;50(5):225. doi:10.1007/s11082-018-1484-2

[14] Wang BX, Wang LL, Wang GZ, et al. A simple design of ultra-broadband and polarization insensitive terahertz metamaterial absorber. Appl Phys A. 2014;115(4):1187–1192. doi:10.1007/s00339-013-8158-5
[15] Xiong H, Hong JS, Luo CM, et al. An ultrathin and broadband metamaterial absorber using multilayer structures. J Appl Phys. 2013;114(6):OP181. doi:10.1063/1.4818318
[16] Karaaslan M, Bamanc M, Ünal E, et al. Broad band metamaterial absorber based on wheel resonators with lumped elements for microwave energy harvesting. Opt Quantum Electron. 2018;50(5):225. doi:10.1007/s11082-018-1484-2
[17] Xu G, Huang J, Ju Z, et al. A novel six-band polarization-insensitive metamaterial absorber with four multiple-mode resonators. Prog Electromagn Res C. 2017;77:133–144. doi:10.2528/PIERC17060203
[18] Deng G, Lv K, Sun H, et al. An ultra-broadband and optically transparent metamaterial absorber based on multilayer indium-tin-oxide structure. J Phys D Appl Phy. 2021;54(16): doi:10.1088/1361-6463/abdb6a
[19] Deng G, Chen W, Yu Z, et al. 3D-printed dielectric-resonator-based ultra-broadband microwave absorber using water substrate. J Electron Mater. 2022;51:2221–2227. doi:10.1007/s11664-022-09439-4
[20] Kourtzanidis K, Pederson DM, Raja LL. Electromagnetic wave energy flow control with a tunable and reconfigurable coupled plasma split-ring resonator metamaterial: a study of basic conditions and configurations. J Appl Phys. 2016;119(20):204904. doi:10.1063/1.4952575
[21] Kong XR, Zhang HF, Dao RN, et al. A tunable polarization insensitive ultra-broadband absorber based on the plasma metamaterial. Opt Commun. 2019;453:124435.
[22] Joozdani MZ, Amirhosseini MK. Wideband absorber with combination of plasma and resistive frequency selective surface. IEEE Trans Plasma Ence. 2016;(12):1–8.
[23] Hua M, et al. Ultra-thin quadri-band metamaterial absorber based on spiral structure. Appl Phys A. Mater Sci Process. 2015;118(2):443–447. doi:10.1007/s00339-014-8766-8
[24] Shi S, Qiao X, Jia Q. A compact ultra-broadband metamaterial absorber for Ku-, K-, and Ka- band applications. Phys Scr. 2021;96(12):125522. doi:10.1088/1402-4896/ac2efa
[25] Jiang H, Yang W, Li R, et al. A conformal metamaterial-based optically transparent microwave absorber with high angular stability. IEEE Antennas Wirel Propag Lett. 2021;(99):1–1.
[26] Huang X, Yang H, Yu S, et al. Triple-band polarization-insensitive wide-angle ultra-thin planar spiral metamaterial absorber. J Appl Phys. 2013;113(21):788. doi:10.1063/1.4809655
[27] Kong X K, Li H M, Bian BR, et al. Microwave tunneling in heterostructures with electromagnetically induced transparency-like metamaterials based on solid state plasma. Eur Phys J Appl Phys. 2016;74(3.
[28] Shen Y, Pei Z, Pang Y, et al. Phase random metasurfaces for broadband wide-angle radar cross section reduction. Microw Opt Technol Lett. 2015;57(12):2813–2819. doi:10.1002/mop.29444
[29] Kalraiya S, Ameen M, Chaudhary RK, et al. Compact ultrathin conformal metamaterial dual-band absorber for curved surfaces. Int J RF Microw Comput-Aided Eng. 2019;29(12): doi:10.1002/mmce.21929
[30] Shen G, Ming Z, Ji Y, et al. Broadband terahertz metamaterial absorber based on simple multi-ring structures. AIP Adv. 2018;8(7):075206. doi:10.1063/1.5024606
[31] He F, Si K, Zha D, et al. Broadband microwave absorption properties of a frequency-selective surface embedded in a ptterned honeycomb absorber. IEEE Trans Electromagn Compat. 2021;xx(99):1–5.
[32] Huang XJ, He L, et al. Water-injected all-dielectric ultra-wideband and prominent oblique incidence metamaterial absorber in microwave regime. J Phys D: Appl Phys. 2017;50(38):385304. doi:10.1088/1361-6463/aa81af
[33] Jiang SC, Xiong X, Hu YS, et al. Controlling the polarization state of light with a dispersion-free metastructure. Phys Rev X. 2014;4(2):021026. doi:10.1103/PhysRevX.4.021026
[34] Weiren Z, Ivan D, et al. Multiband coherent perfect absorption in a water-based metasurface. Opt Express; 25(14):15737–15745.
[35] Song Z, Kai W, Li J, et al. Broadband tunable terahertz absorber based on vanadium dioxide metamaterials. Opt Express. 2018;26(6):7148. doi:10.1364/OE.26.007148

[36] Huang J, Li J, Yang Y, et al. Active controllable dual broadband terahertz absorber based on hybrid metamaterials with vanadium dioxide. Opt Express. 2020;28(5.
[37] Kim DS, Kim DH, Hwang S, et al. Broadband terahertz absorber realized by self-assembled multilayer glass spheres. Opt Express. 2012;20(12):13566–13572. doi:10.1364/OE.20.013566
[38] Liu YC, Qian YX, Hu FR, et al. A dynamically adjustable broadband terahertz absorber based on a vanadium dioxide hybrid metamaterial. Results Phys. 2020;19:103384.
[39] Xu HX, Wang GM, Qi MQ, et al. Triple-band polarization-insensitive wide-angle ultra-miniature metamaterial transmission line absorber. Phys Rev B. 2012;86(20):205104. doi:10.1103/PhysRevB.86.205104
[40] Xu HX, Wang M, Hu G, et al. Adaptable invisibility management using kirigami-inspired transformable metamaterials. Research. 2022;1:11.
[41] Wang C, Xu HX, Wang Y, et al. Heterogeneous amplitudephase metasurface for distinct wavefront manipulation. Adv Photonics Res. 2021;2(10):2100102. doi:10.1002/adpr.202100102
[42] Wang YZ, Xu HX, Wang CH, et al. Multimode-assisted broadband impedance-gradient thin metamaterial absorber. Adv Photonics Res. 2022;3(10):2200063. doi:10.1002/adpr.202200063
[43] Huang S, Xie Z, Chen W, et al. Metasurface with multi-sized structure for multi-band coherent perfect absorption. Opt Express. 2018;26(6):7066. doi:10.1364/OE.26.007066
[44] Karaaslan M, Bağmancı M, Ünal E, et al. Broad band metamaterial absorber based on wheel resonators with lumped elements for microwave energy harvesting. Opt Quantum Electron. 2018;50:225.
[45] Yi D, Wei XC, Xu YL. Tunable microwave absorber based on patterned graphene. IEEE Trans Microwave Theory Tech. 2017;(99):1–8.
[46] Wang Y, Yue L, Cui Z, et al. Optically tunable single narrow band all-dielectric terahertz metamaterials absorber. AIP Adv. 2020;10(4):045039. doi:10.1063/5.0003817
[47] Zhang J, Wang G, Zhang B, et al. Photo-excited broadband tunable terahertz metamaterial absorber. Opt Mater. 2016;54:32–36. doi:10.1016/j.optmat.2016.02.011